


RESEARCH ARTICLE | JANUARY 18 2024

# One-step model photoemission calculations of Type-II Dirac semimetal $\text{PtTe}_2$

Muthu Masilamani ; Jakub Schusser; Mohammed Qahosh; Lukasz Plucinski; Friedrich Reinert




*AIP Conf. Proc.* 3054, 070004 (2024)


<https://doi.org/10.1063/5.0187969>




10 April 2024 11:45:02



Lock-in Amplifier



Boxcar Averager



Zurich  
Instruments

Find out more

Boost Your Optics and  
Photonics Measurements

# One-Step Model Photoemission Calculations of Type-II Dirac Semimetal PtTe<sub>2</sub>

Muthu Masilamani<sup>1, a)</sup>, Jakub Schusser<sup>1</sup>, Mohammed Qahosh<sup>2</sup>, Lukasz Plucinski<sup>2</sup> and Friedrich Reinert<sup>1</sup>

<sup>1</sup>*Experimentelle Physik VII and Würzburg-Dresden Cluster of Excellence ct.qmat, Universität Würzburg, D97074 Würzburg, Germany*

<sup>2</sup>*Peter Grünberg Institut (PGI-6), Forschungszentrum Jülich GmbH, Jülich, Germany*

<sup>a)</sup> Corresponding author: muthu.masilamani@physik.uni-wuerzburg.de

**Abstract.** Among the class of transition metal dichalcogenides (TMDC) PtTe<sub>2</sub> with trigonal structure belongs to type-II Dirac semimetals and attracted extensive research interest due to the Dirac points appearing at the band touching points of electron and hole pockets. Here we have studied photoelectrons from the surface and bulk states of PtTe<sub>2</sub> using state-of-the-art photoemission theory and experiment. We used theoretical photoemission model to distinguish between surface and bulk Dirac states through determinant criterion using the one-step model of the photoemission within the spin-polarized relativistic Korringa-Kohn-Rostoker (SPR-KKR) Green's function method.

## INTRODUCTION

In topological semimetals the valence and conduction bands touch only at discrete points (Dirac or Weyl) and disperse linearly in all directions around these points [1]. In a Dirac semimetal (DSM) or Weyl semimetal (WSM), such degeneracies between valence and conduction bands give rise to low energy excitations-Dirac fermions described by the massless Dirac equation [2,3]. The electronic energy dispersion relation of such semimetals can be generically expressed as  $E(\mathbf{k}) = T(\mathbf{k}) \pm U(\mathbf{k})$ , where  $T(\mathbf{k})$  and  $U(\mathbf{k})$  are potential and kinetic energy terms respectively [4]. In type-I semimetals,  $T(\mathbf{k}) < U(\mathbf{k})$  and the Dirac or Weyl points appear at the Fermi energy with linear dispersion in all directions. In type-II semimetals,  $T(\mathbf{k}) > U(\mathbf{k})$  and the Dirac cone gets tilted over the provided momentum direction in the Brillouin zone (BZ) and emerges at the topologically protected band touching points of valence and conduction bands [5]. A Dirac point separates into Weyl points if either inversion or time-reversal symmetry is broken [6]. Here we distinguish Dirac state from bulk state in PtTe<sub>2</sub> using angle-resolved photoemission spectroscopy (APRES) experiment and one-step model photoemission calculations.

Platinum ditelluride is a Dirac semimetal and crystallizes in the space group P3m1 (No. 164) with lattice constants  $a = b = 4.05 \text{ \AA}$  and  $c = 5.48 \text{ \AA}$ . The three-atom-layered structure of PtTe<sub>2</sub> is composed of a sublayer of Pt sandwiched between two sublayers of Te (Fig.1(a)). The bulk BZ and projected hexagonal surface BZ onto the (001) plane is shown in Fig.1(b). The single crystal PtTe<sub>2</sub> was purchased from HQ Graphene and the electronic states in BZ were localized using ARPES with HIS13 helium discharge lamp as He-I photon source and MB scientific A1 hemispherical electron analyser.

We established a good correspondence between ARPES theory and experiment through systematic study of bulk and surface states of PtTe<sub>2</sub> using the SPR-KKR band structure software package [7] and ARPES experiment. This package is based on the Green's function and multiple scattering formalism. It properly describes the photoemission matrix-element by including all the experimental parameters such as photon energy, light polarization and geometry

configurations. Reliability of SPR-KKR in terms of reproducing expected matrix element behavior was established both in the context of TMDC of the space group (No.164) as  $\text{PtTe}_2$  [8,9] but also other space groups [10–12].

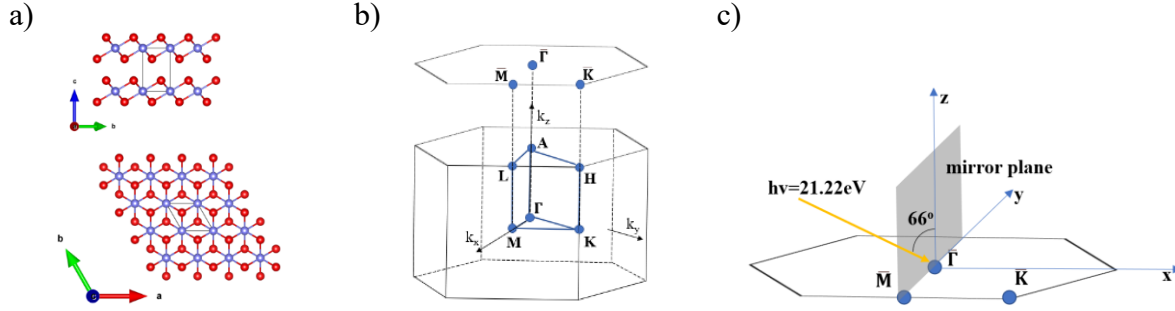


**FIGURE 1.** (a) Side and top view of  $\text{PtTe}_2$  lattice structure. Blue and red balls represent Pt atoms and Te atoms respectively. The black rectangle indicates unit cell. (b) Bulk and projected surface Brillouin zone onto (001) surface. (c) Experimental geometry.

## ONE-STEP MODEL OF PHOTOEMISSION CALCULATIONS

Our spin- and angle-resolved photoemission data were augmented by the one-step model of the photoemission within the spin-polarized relativistic Korringa-Kohn-Rostoker (SPR-KKR) Green's function method of the Munich band structure software package [7]. We used local density approximation (LDA) for computing the exchange-correlation potential. The spin-orbit coupling (SOC) is treated using the fully relativistic Dirac equation which makes the photoemission matrix element spin dependent through relativistic dipole selection rules [13,14]. The bulk potential is computed using the self-consistent full-potential linear muffin-tin orbital (FP-LMTO) method. The KKR equations are solved with an angular momentum cutoff of  $l_{\text{max}} = 4$  [15]. The finite lifetime effects in the initial state and final states have been included by adding a constant imaginary part to the local DFT potential  $V_o(E) = V_{or}(E) + iV_{oi}(E)$  [16]. We choose  $iV_{oi}(E_2) = 1.00 \text{ eV}$  and  $iV_{oi}(E_1) = 0.05 \text{ eV}$  for the final and initial states respectively. After checking the layer and  $\mathbf{G}$ -vector convergence [17], the surface barrier (SFB) parameter is tuned to match with the experiment. We used Rundgren-Malmström (RM) surface barrier model [18] to ensure smooth transition between Coulomb-like image potential on the vacuum side far outside the crystal surface and the bulk crystal potential [16]. The multiple scattering formalism is considered for a wavefunction between the topmost layer of the semi-infinite bulk crystal and the RM barrier and the corresponding reflection matrices  $\mathbf{R}_b$  and  $\mathbf{R}_v$  are calculated. The bulk reference energy  $V_{or}$  is connected to the asymptotic regime  $\sim 1/z$  by the surface potential. In Fig.2 we see evolution of band structure of  $\text{PtTe}_2$  as a function of SFB parameter. As the SFB parameter influences mainly the energy dispersion of surface states because of its direct localization at the surface, the qualitative changes in the band dispersion can be attributed mostly to the surface states.

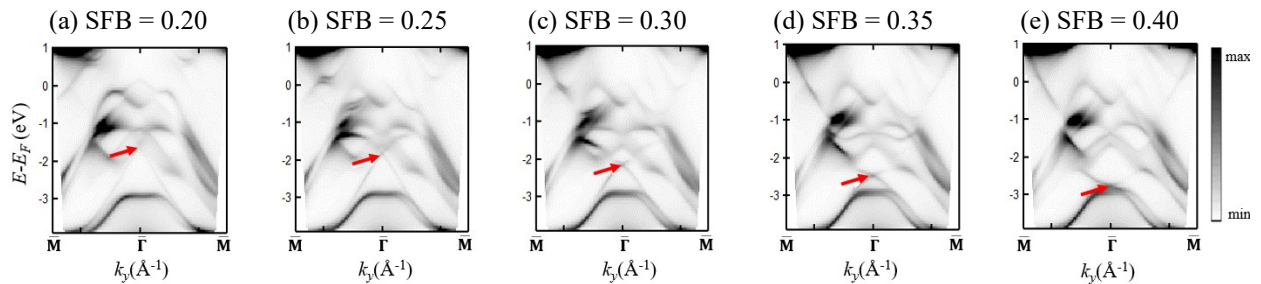


**FIGURE 2.** A series of calculated  $E$  vs  $k_y$  plots with varying SFB. We see certain bands responds to the SFB indicating they are surface origin. The Dirac point (red arrow) shifts (from 1.8189 eV to 2.7623 eV) with respect to SFB (from 0.20 to 0.40) indicating it is surface Dirac state.

It should be noted that the SPR-KKR package has access to the photoelectrons emitted from the states above the Fermi level (Fig.2) which are not accessible by the conventional ARPES experiment. For the classification of bulk states (BS) and surface states (SS), we employ determinant criterion method [19,20]. This method provides qualitatively similar information to changing the SFB parameter. The presence of a surface state is indicated by  $|\det(\mathbf{I} - \mathbf{R}_v \mathbf{R}_b)|$  approaching zero. The bulk character of a state is directly proportional to the  $|\det(\mathbf{I} - \mathbf{R}_v \mathbf{R}_b)|$ .

With fine tuning of all these parameters and using the same experimental geometry with s-polarized light of energy 21.22 eV (He-I line), we quantitatively mapped majority of the experimental dispersive features using the one-step model photoemission calculations (Fig.3). It should also be noted that in order to map these features, the theoretical spectra were renormalized in energy by a factor of 1.21. A Dirac cone is situated at  $E-E_F = -2.25$  eV below the Fermi level (Fig. 3 (a-c)) which has been identified as a topological surface state (TSS) in PtSe<sub>2</sub> class of TMDC [4,21–23]. A type-II bulk Dirac cone at the binding energy  $\sim 0.5$  eV below the Fermi level and the surface states between  $-0.5$  eV to  $-1$  eV are in good agreement with [4]. In contrast to [22], where the TSS is identified at binding energy  $\sim 1$  eV below the Fermi level, our calculation indicates that this state has bulk-like character (Fig.3(a)).

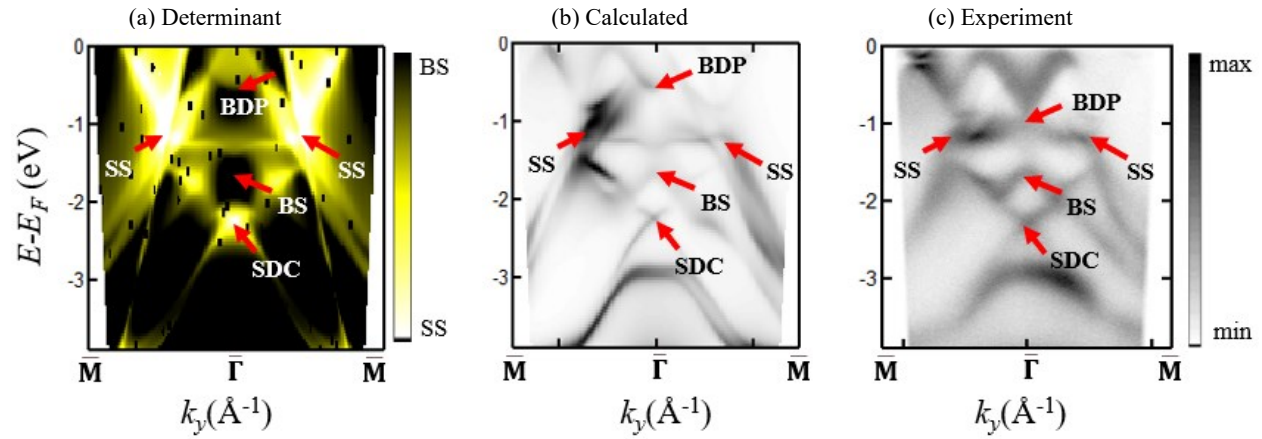


**FIGURE 3.** (a) The  $E$  vs  $k_y$  plot of the corresponding determinant criterion. (b) and (c) Calculated and experimental  $E$  vs  $k_y$  intensity plot along M- $\Gamma$ -M direction. The surface Dirac state is localized at the  $\Gamma$ -point with binding energy of  $-2.25$  eV. The determinant criterion qualitatively localizes the SS observed by probing SFB parameter.

The surface Dirac cone (SDC) is revealed in Fig.4 through the corresponding constant energy  $k_x$ - $k_y$  cuts at binding energies ( $-2.3$  eV to  $-2.5$  eV) in Brillouin zone with the  $\Gamma$ -point as the center (Fig.4). The determinant criterion indicates bulk origin of the bands in the vicinity of SDC. The experimental ARPES maps were taken using unpolarized He-I light whereas the theoretical ARPES spectral function were calculated by using s-polarized He-I light. Due to this difference in the polarization of light used, the one-to-one correspondence between experimental and theoretical photoemission spectra should not be expected.

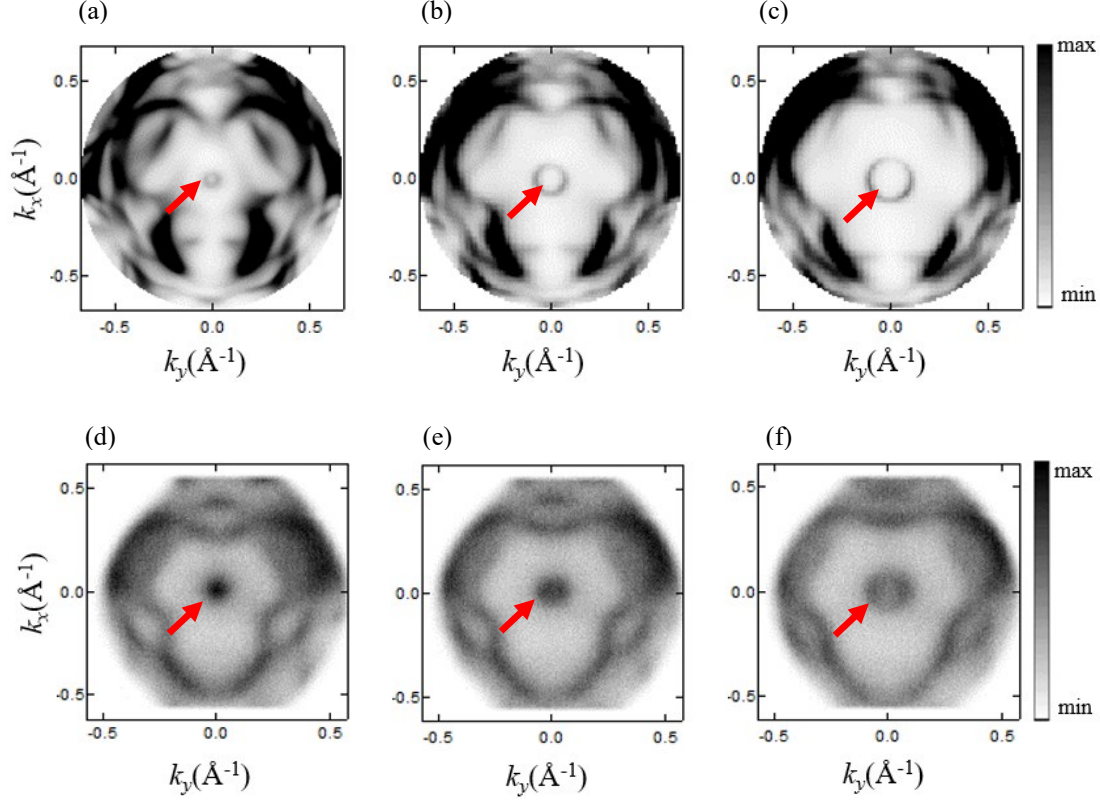


**FIGURE 4.** Tracking of SDC. Series of constant energetic  $k_x$ - $k_y$  cuts obtained through ARPES calculation (a-c) and experiment (d-f) at binding energy correspondingly starting from binding energy  $-2.3\text{eV}$  to  $-2.5\text{eV}$  with the step size of  $0.1\text{eV}$ . The red arrow indicates the position of the SDC with radius of cross-section ranging from  $5.92 \times 10^{-2} \text{ \AA}^{-1}$  to  $2.13 \times 10^{-1} \text{ \AA}^{-1}$  respectively from (a) to (c).

## CONCLUSION

In this work we created a model which quantitatively transcribe most of the features in the band structure mapped by experimental ARPES. Moreover, we have shown that surface states and bulk states can be differentiated by using the surface barrier parameter and determinant criterion within the SPR-KKR package. Previously, it was claimed that the TSS at  $\sim 1 \text{ eV}$  below the Fermi level in  $1\text{T-PdTe}_2$ , a sister compound of  $1\text{T-PtTe}_2$ , has a surface character [22]. Our calculations, however, confirm that this state has bulk character. Moreover, our theoretical model of  $1\text{T-PtTe}_2$  will serve as the basis for future studies of asymmetries in measured spin texture which are induced by the experimental geometry [24] and the spin-orbital texture mapping from the spin- and angle- resolved photoemission.

## ACKNOWLEDGEMENT

This work was funded by the Würzburg-Dresden Cluster of Excellence on Complexity and Topology in Quantum Matter—ct.qmat (EXC 2147, project-id 390 858 490) and by the DFG through SFB1170 “Tocotronics,” RE 1469/ 13-2. We also thank Professor Ján Minár for letting us use the infrastructure of the computation cluster at New Technologies Research Centre, Pilsen, Czech Republic. L.P and M.Q acknowledge funding for this project from the Palestinian-German Science Bridge financed by the German Federal Ministry of Education and Research.

## REFERENCES

1. Z. K. Liu, B. Zhou, Y. Zhang, Z. J. Wang, H. M. Weng, D. Prabhakaran, S.-K. Mo, Z. X. Shen, Z. Fang, X. Dai, Z. Hussain, and Y. L. Chen, "Discovery of a Three-Dimensional Topological Dirac Semimetal, Na<sub>3</sub>Bi," *Science* **343**, 864–867 (2014).
2. A. H. Castro Neto, F. Guinea, N. M. R. Peres, K. S. Novoselov, and A. K. Geim, "The electronic properties of graphene," *Rev. Mod. Phys.* **81**, 109–162 (2009).
3. S. M. Young, S. Zaheer, J. C. Y. Teo, C. L. Kane, E. J. Mele, and A. M. Rappe, "Dirac Semimetal in Three Dimensions," *Phys. Rev. Lett.* **108**, 140405 (2012).
4. M. Yan, H. Huang, K. Zhang, E. Wang, W. Yao, K. Deng, G. Wan, H. Zhang, M. Arita, H. Yang, Z. Sun, H. Yao, Y. Wu, S. Fan, W. Duan, and S. Zhou, "Lorentz-violating type-II Dirac fermions in transition metal dichalcogenide PtTe<sub>2</sub>," *Nat Commun* **8**, 257 (2017).
5. A. A. Soluyanov, D. Gresch, Z. Wang, Q. Wu, M. Troyer, X. Dai, and B. A. Bernevig, "Type-II Weyl semimetals," *Nature* **527**, 495–498 (2015).
6. S. Murakami, "Phase transition between the quantum spin Hall and insulator phases in 3D: emergence of a topological gapless phase," *New J. Phys.* **9**, 356 (2007).
7. H. Ebert, D. Ködderitzsch, and J. Minár, "Calculating condensed matter properties using the KKR-Green's function method—recent developments and applications," *Rep. Prog. Phys.* **74**, 096501 (2011).
8. S. Beaulieu, M. Schüler, J. Schusser, S. Dong, T. Pincelli, J. Maklar, A. Neef, F. Reinert, M. Wolf, L. Rettig, J. Minár, and R. Ernstorfer, "Unveiling the orbital texture of 1T-TiTe<sub>2</sub> using intrinsic linear dichroism in multidimensional photoemission spectroscopy," *npj Quantum Mater.* **6**, 1–11 (2021).
9. Z. El Youbi, S. W. Jung, S. Mukherjee, M. Fanciulli, J. Schusser, O. Heckmann, C. Richter, J. Minár, K. Hricovini, M. D. Watson, and C. Cacho, "Bulk and surface electronic states in the doped semimetallic HfTe<sub>2</sub>," *Phys. Rev. B* **101**, 235431 (2020).
10. R. Ono, A. Marmodoro, J. Schusser, Y. Nakata, E. F. Schwier, J. Braun, H. Ebert, J. Minár, K. Sakamoto, and P. Krüger, "Surface band characters of the Weyl semimetal candidate material MoTe<sub>2</sub> revealed by one-step angle-resolved photoemission theory," *Phys. Rev. B* **103**, 125139 (2021).
11. S. Beaulieu, J. Schusser, S. Dong, M. Schüler, T. Pincelli, M. Dendzik, J. Maklar, A. Neef, H. Ebert, K. Hricovini, M. Wolf, J. Braun, L. Rettig, J. Minár, and R. Ernstorfer, "Revealing Hidden Orbital Pseudospin Texture with Time-Reversal Dichroism in Photoelectron Angular Distributions," *Phys. Rev. Lett.* **125**, 216404 (2020).
12. M. Fanciulli, J. Schusser, M.-I. Lee, Z. E. Youbi, O. Heckmann, M. C. Richter, C. Cacho, C. Spezzani, D. Bresteau, J.-F. Hergott, P. D'Oliveira, O. Tcherbakoff, T. Ruchon, J. Minár, and K. Hricovini, "Spin, time, and angle resolved photoemission spectroscopy on WTe<sub>2</sub>," *Phys. Rev. Research* **2**, 013261 (2020).
13. E. Pavarini, E. Koch, D. Vollhardt, A. I. Lichtenstein, Institute for Advanced Simulation, German Research School for Simulation Sciences, and Deutsche Forschungsgemeinschaft, eds., *DMFT at 25: Infinite Dimensions: Lecture Notes of the Autumn School on Correlated Electrons 2014: At Forschungszentrum Jülich 15-19 September 2014*, Schriften Des Forschungszentrums Jülich. Reihe Modeling and Simulation No. Band 4 (Forschungszentrum Jülich, Zentralbibliothek, Verl, 2014).
14. J. Braun, "The theory of angle-resolved ultraviolet photoemission and its applications to ordered materials," *Rep. Prog. Phys.* **59**, 1267 (1996).
15. J. Minár, L. Chioncel, A. Perlov, H. Ebert, M. I. Katsnelson, and A. I. Lichtenstein, "Multiple-scattering formalism for correlated systems: A KKR-DMFT approach," *Phys. Rev. B* **72**, 045125 (2005).
16. J. Braun and M. Donath, "Contest between surface resonances and surface states at 3 *d* ferromagnets," *Europhys. Lett.* **59**, 592–598 (2002).
17. V. Strocov, L. Lev, F. Alarab, P. Constantinou, T. Schmitt, T. Stock, L. Nicolaï, J. Ocenasek, and J. Minar, *Are High-Energy Photoemission Final States Free-Electron-Like?* (In Review, 2023).
18. G. Malmström and J. Rundgren, "A program for calculation of the reflection and transmission of electrons through a surface potential barrier," *Computer Physics Communications* **19**, 263–270 (1980).
19. J. Braun, C. Math, A. Postnikov, and M. Donath, "Surface resonances versus surface states on Fe(110)," *Phys. Rev. B* **65**, 184412 (2002).



20. J. Schusser, H. Bentmann, M. Ünzelmann, T. Figgemeier, C.-H. Min, S. Moser, J. N. Neu, T. Siegrist, and F. Reinert, "Assessing Nontrivial Topology in Weyl Semimetals by Dichroic Photoemission," *Phys. Rev. Lett.* **129**, 246404 (2022).
21. M. S. Bahramy, O. J. Clark, B.-J. Yang, J. Feng, L. Bawden, J. M. Riley, I. Marković, F. Mazzola, V. Sunko, D. Biswas, S. P. Cooil, M. Jorge, J. W. Wells, M. Leandersson, T. Balasubramanian, J. Fujii, I. Vobornik, J. E. Rault, T. K. Kim, M. Hoesch, K. Okawa, M. Asakawa, T. Sasagawa, T. Eknapakul, W. Meevasana, and P. D. C. King, "Ubiquitous formation of bulk Dirac cones and topological surface states from a single orbital manifold in transition-metal dichalcogenides," *Nature Mater* **17**, 21–28 (2018).
22. O. J. Clark, M. J. Neat, K. Okawa, L. Bawden, I. Marković, F. Mazzola, J. Feng, V. Sunko, J. M. Riley, W. Meevasana, J. Fujii, I. Vobornik, T. K. Kim, M. Hoesch, T. Sasagawa, P. Wahl, M. S. Bahramy, and P. D. C. King, "Fermiology and Superconductivity of Topological Surface States in PdTe<sub>2</sub>," *Phys. Rev. Lett.* **120**, 156401 (2018).
23. Y. Liu, J.-Z. Zhao, L. Yu, C.-T. Lin, A.-J. Liang, C. Hu, Y. Ding, Y. Xu, S.-L. He, L. Zhao, G.-D. Liu, X.-L. Dong, J. Zhang, C.-T. Chen, Z.-Y. Xu, H.-M. Weng, X. Dai, Z. Fang, and X.-J. Zhou, "Identification of Topological Surface State in PdTe<sub>2</sub> Superconductor by Angle-Resolved Photoemission Spectroscopy\*," *Chinese Phys. Lett.* **32**, 067303 (2015).
24. T. Heider, G. Bihlmayer, J. Schusser, F. Reinert, J. Minár, S. Blügel, C. M. Schneider, and L. Plucinski, "Geometry-Induced Spin Filtering in Photoemission Maps from WTe<sub>2</sub> Surface States," *Phys. Rev. Lett.* **130**, 146401 (2023).